



PAPER • OPEN ACCESS

Multilayering BZO nanocolumns with different defect densities for YBCO high field applications

To cite this article: Moe M Aye *et al* 2021 *New J. Phys.* **23** 113031

View the [article online](#) for updates and enhancements.

You may also like

- [High critical current density over 1 MA cm² at 13 T in BaZrO₃ incorporated Ba\(Fe,Co\)₂As₂ thin film](#)
Jongmin Lee, Jianyi Jiang, Fumitake Kametani *et al.*
- [New insight into strain and composition of BaZrO₃ nanorods in REBCO superconductor](#)
Goran Majkic, Jong Seok Jeong, Hwanhui Yun *et al.*
- [Optimal Nanod defect Configurations via Strain-Mediated Assembly for Optimized Vortex-Pinning in Superconducting Wires from 5K-77K](#)
A. Goyal and S. H. Wee



PAPER

Multilayering BZO nanocolumns with different defect densities for YBCO high field applications

OPEN ACCESS

RECEIVED
22 August 2021REVISED
21 October 2021ACCEPTED FOR PUBLICATION
4 November 2021PUBLISHED
22 November 2021

Original content from
this work may be used
under the terms of the
[Creative Commons
Attribution 4.0 licence](#).

Any further distribution
of this work must
maintain attribution to
the author(s) and the
title of the work, journal
citation and DOI.

Moe M Aye^{1,2,*} , Elmeri Rivasto^{1,2} , Mukarram Z Khan^{1,2} , H Rijckaert³ ,
H Palonen¹, H Huhtinen¹ , Isabel Van Driessche³ and P Paturi¹ ¹ Wihuri Physical Laboratory, Department of Physics and Astronomy, University of Turku, 20014 Turku, Finland² University of Turku Graduate School (UTUGS), University of Turku, 20014 Turku, Finland³ SCRiPTS, Department of Chemistry, Ghent University, 9000 Ghent, Belgium

* Author to whom any correspondence should be addressed.

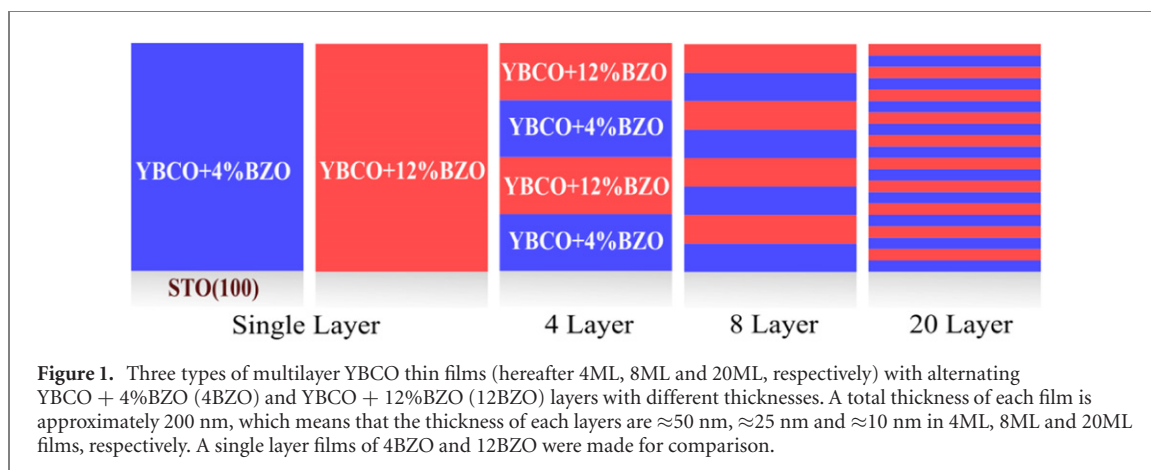
E-mail: moe.m.aye@utu.fi**Keywords:** HTS superconductors, BZO doped YBCO, multilayered film, flux pinningSupplementary material for this article is available [online](#)**Abstract**

The multilayer structures of alternating superconducting YBCO films doped with different BZO nanocolumn densities were utilized. We show that using 50 nm thick layers increases J_c in the whole angular range by maximum 40% as compared with 200 nm single layer BZO-doped or multilayers with smaller thickness. Multilayering is found to be most effective at high magnetic fields and temperatures. These results indicate that demonstrated multilayer structures are extremely attractive for various electrical power applications in the foreseeable future. The experimental outcomes are thoroughly discussed with the mechanisms of crystalline quality and flux pinning in YBCO with different BZO nanorod densities multilayers of varying thicknesses.

1. Introduction

Maximizing critical current density (J_c) and minimizing its anisotropy in YBCO thin films and coated conductors has drawn tremendous attention in high temperature superconductor (HTS) research [1–3]. In the practical applications, HTS needs to maximize their self-field and in-field performance to achieve the highest J_c at the desired temperatures required for the electrical power applications such as large motor (4–5 T, 20–77 K), generator (4–5 T, 20–50 K), fault current limiter (0.1–3 T, 20–77 K) and superconducting magnetic energy storage (5–10 T, 20–77 K) [3]. To meet these requirements and to make HTS materials attractive for various kinds of applications, controlling the morphology, dimension, orientation and concentration of artificial pinning centers (APC) in the YBCO matrix is necessary [4–8]. Several approaches have been successfully developed to optimize the pinning architecture that composes of different types of flux pinning structures such as 1D, 2D and 3D APCs in epitaxial APC/YBCO films [9–13]. In addition to mixing APCs with YBCO, a great interest has been addressed to multilayer structures, where APC-free YBCO layers were tailored together with layers of YBCO containing APCs [10, 14–18].

Great improvement in flux pinning properties has been achieved in YBCO multilayer films, where different secondary phase layers such as $\text{YBa}_2\text{Cu}_3\text{O}_5$ [17], Y_2O_3 [19–23], CeO_2 [18, 24], BaZrO_3 (BZO) [25, 26], were grown together with YBCO layers. In addition, an exciting progress has been made on alternating APC-free YBCO layers with APC-added YBCO layers for example YBCO with YBCO/BZO [27–29], and YBCO with YBCO/ BaSnO_3 (BSO) [30]. Especially, particular interest has been expressed to the formation of self-assembled nanorods that have been observed being of unmatched quality, much more effective than the other types of APCs and especially all the naturally formed pinning centers [6, 9, 11, 31–40]. For instance, significant improvement in the pinning properties has been demonstrated by multilayering the BZO doped YBCO with CeO_2/YBCO [28, 29], $\text{YBCO} + \text{Y}_2\text{O}_3$ [41] and BaCeO_3 (BCO) doped YBCO [42]. It has also been shown that multilayered BZO doped YBCO with CeO_2/YBCO interlayer can result in both c -axis oriented columnar and along the ab -plane oriented defects [28, 29]. Also, short



BZO nanorods with the YBCO matrix together with the BCO nanodot layers have been suggested as a multilayer structure that improves pinning capability throughout the whole angular range when compared with the cases of multilayer architectures having APC-free YBCO between the YBCO layers with BZO nanorods [42].

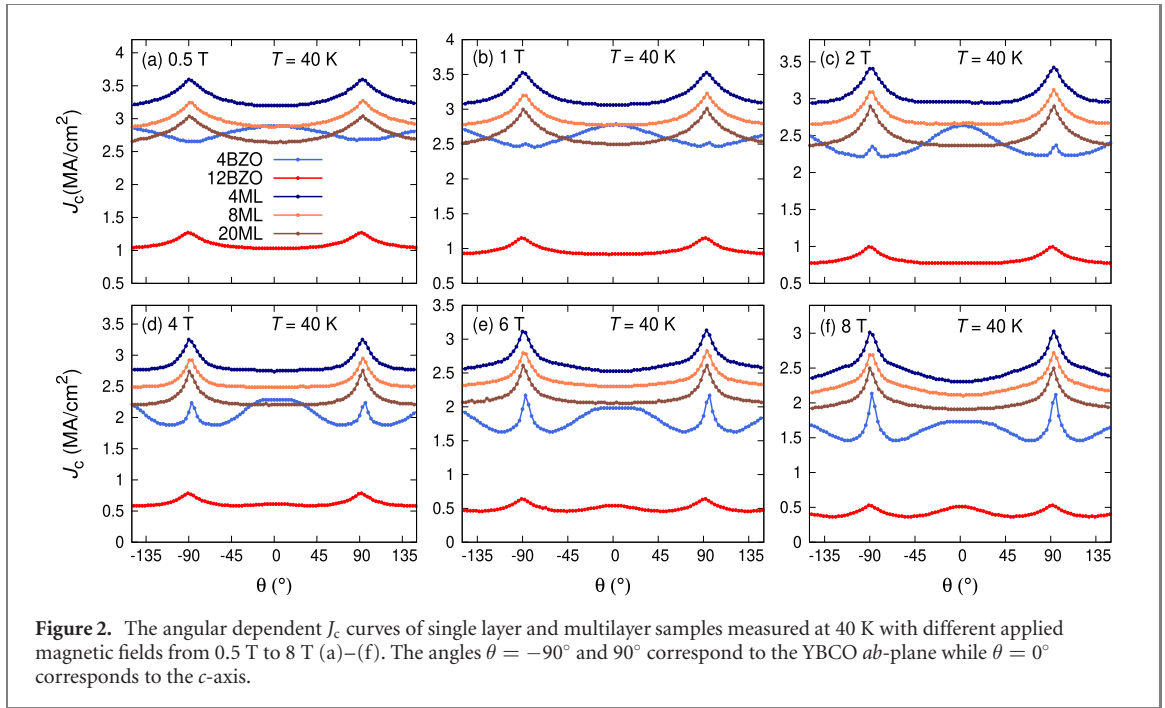
In general, when trying to optimize J_c at high magnetic field (B), the best possible combination between $J_c(0)$ and $J_c(B)$ should be fulfilled [3, 43]. The attempt reaching the depairing current by only trying to affect the coherence length and penetration depth of the superconductor by increasing the electron mean free path is not only the limiting factor, since the J_c at high fields is mainly determined by the vortex pinning properties such as the pinning force and the irreversibility field [3, 43, 44]. Therefore, by optimizing the nanorod diameter and their density and distribution seems to be the most important factor when finding the optimal pinning landscape for different magnetic field and temperature ranges [12, 14, 38, 45, 46]. However, in previous multilayer combinations, the nanorod density has not been varied and thus the understanding in this respect is inadequate. Especially, since the APC-free and defect-free YBCO as an alternating middle layer certainly increases the effective mean free path of electrons, but at the same time leaves these layers entirely redundant in terms of trapping the vortices.

In this work, in order to optimize the flux pinning properties for various power applications working at magnetic fields around 3–5 T, we have deposited the multilayer structures with various thicknesses by alternating the BZO doped YBCO layers with different BZO concentrations. The multilayers are structurally, magnetically and resistively characterized and the results are compared and discussed with the YBCO single layer films doped with 4% and 12% BZO nanorods.

2. Methods

The YBCO films doped with 4 wt.% and 12 wt.% BZO (hereafter 4BZO and 12BZO, respectively) were prepared together with a set of multilayer films, consisting of alternating 4BZO and 12BZO layers on SrTiO₃(100) substrate by pulsed laser deposition (PLD) as illustrated in figure 1. The BZO doped YBCO targets were prepared by a solid state reaction method and the details of preparation are described elsewhere [47]. The multilayer structures consisted of alternating layers of 4BZO and 12BZO with total of 4, 8 and 20 layers. The total thickness of the films was kept constant, around 200 nm, by shooting a total number of 2000 pulses [48]. In order to get the respective target for each sequential layer, the deposition was stopped for around 120 s during which the PLD target was changed *in situ* [25]. The substrate temperature of 750 °C in oxygen partial pressure of 175 mTorr were kept constant during the deposition of the film using a XeCl excimer laser ($\lambda = 308$ nm) with 1.3 J cm⁻² laser energy density and 5 Hz repetition frequency. After the deposition, the films were cooled from 750 °C to 725 °C and *in situ* annealed in oxygen at 750 Torr for 10 min. All the films were grown by PLD in previously optimized deposition conditions and the further details of the PLD system together with deposition parameters have been given elsewhere [35].

Detailed structural characterizations such as in-plane and out-of-plane crystallographic properties were determined by x-ray diffraction (XRD) measurements with a Philips Empyrean system. The microstructure of the films, including the size and distribution of the nanocolumns and stacking faults (SFs), were investigated with Cs-corrected JEOL JEM 2200-FS scanning transmission electron microscopy operated at 200 kV with bright-field (BF-STEM) detector. Cross-sectional lamellae were prepared by a focused ion beam in an FEI Nova 600 Nanolab Dual Beam scanning electron microscopy (FIB-SEM) and extracted using the *in situ* lift-out procedure with an Omniprobe extraction needle [49].



The magnetic measurements were made with a quantum design physical property measurement system (PPMS). Ac magnetization measurements were carried out to determine the superconducting critical temperatures, T_c , and the J_c as a function of B which were calculated from the opening of the measured hysteresis loop according to the Bean model [50]. Hysteresis loops were measured up to 8 T by dc magnetization measurement with PPMS ACMS II system. Transport J_c measurements were carried out by a standard four-probe technique. Before the measurement, microbridges with 50 μm wide current stripes were formed on the film by photolithography and aluminum wire contact was made by TPT HB05 Wire Bonder. The anisotropic critical current values ($J_c(\theta)$) were measured at 10 K, 40 K, 50 K, and 65 K under a wide magnetic field range of 0.5, 1, 2, 4, 6, 8 T with θ varying from 0° to 360° angular range using 3° of step with a horizontal rotator option available in PPMS.

3. Experimental results

3.1. The effect of multilayering on critical current density

The contribution of flux pinning in deposited films were characterized by their superconducting properties that were obtained through angular dependence $J_c(B, \theta)$ measurements at 40 K with a wide range of magnetic field ($B = 0.5, 1, 2, 4, 6, 8$ T). Figures 2(a)–(f) show $J_c(\theta)$ curves for single layer 4BZO and 12BZO films as well as for all the multilayers 4ML, 8ML and 20ML. In the 4BZO film, the prominent c -axis peak is visible in the whole magnetic field range, but it seems to be the most pronounced around 2 T. The peak along the ab -plane in 4BZO increases remarkably when the magnetic field is increased. These are in line with our earlier results, where the correlated pinning along the c -axis is the most effective in the vicinity of the matching field and, on the other hand, the great number of vortices at high fields can also be partially pinned by the SFs along the YBCO ab -plane [51–53]. In 12BZO, the absolute J_c is clearly decreased when compared with the 4BZO film. Although the high BZO concentration increases the number of effective nanorods in terms of flux pinning, the excess APC also diminishes the effective superconducting cross-sectional area of YBCO that also reduces J_c [12, 29]. In addition, the c -axis peak is not visible at low fields in 12BZO, but its increase above 2 T can be understood by the low-field random pinning [5] and the presence of c -axis correlated pinning due to the high nanocolumn density at high fields. This fairly trivial connection is also discussed in SI (<https://stacks.iop.org/NJP/23/113031/mmedia>), where structural and magnetic properties are compared.

In multilayer structures, only a gradual change in $J_c(\theta)$ curves in the vicinity of the ab -direction can be obtained and this is consistent with the earlier studies for multilayer structures [21, 26, 28, 42, 54, 55]. Surprisingly, when compared with the single layer films, the improvement of the absolute $J_c(\theta)$ in multilayer films is significant, even though the c -axis peak is not visible in any of the multilayer structures. This indicates that the multilayering should improve either the intrinsic superconducting properties of YBCO or flux pinning properties over a wide angular range, or both of them. Obviously, the 4ML film has the highest

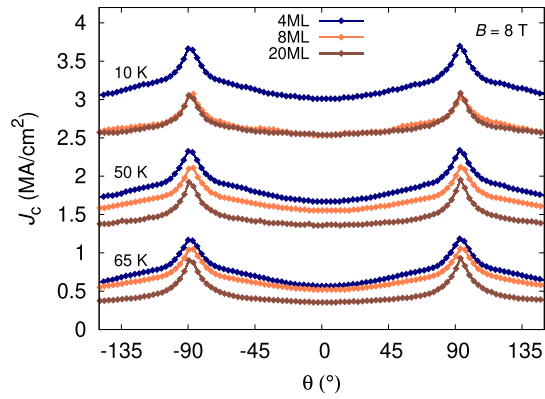


Figure 3. The comparison of the angular dependent J_c of multilayer samples at 10 K, 50 K and 65 K under 8 T field.

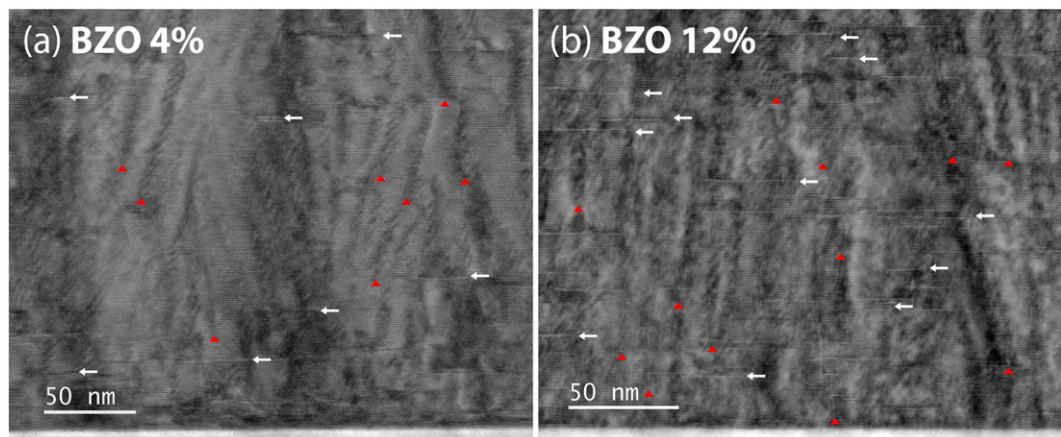


Figure 4. Cross-sectional STEM images of 4 wt.% BZO doped (a) and 12 wt.% BZO doped (b) YBCO films. The white arrows indicate SFs, while the red triangles indicate BZO nanorods.

J_c in the whole magnetic field range and J_c decreases systematically with decreasing layer thickness. When the $J_c(\theta)$ curves are compared with the single layer films of 4BZO and 12BZO, we can assume that the layers with different defect densities might improve the epitaxial growth and thus sustain better film quality in multilayered architectures [24, 25, 28, 54, 56].

Figure 3 shows the temperature evolution of $J_c(\theta)$ measured at 10 K, 50 K and 65 K in 8 T field for all the multilayer structures. At 10 K, J_c curves of 8ML and 20ML films overlap and their $J_c(\theta)$ is clearly smaller in the whole angular range than in the 4ML film. At higher temperatures of 50 K and 65 K, the $J_c(\theta)$ curve of 8ML film starts to moderately approach that of 4ML, which can be attributed to highly improved pinning performance of 8ML film at high temperature, as the films with greater number of layers are expected to contain more effective pinning centers. Moreover, for 20ML film, $J_c(\theta)$ curve starts to diverge again and therefore, we can only conclude that the multilayering works similarly in the whole measured temperature range. This is in line with the theoretical model presented recently [57], where the pinning centers are shown to become increasingly more effective as the temperature is increased.

3.2. Vortex pinning structure

The 4BZO and 12BZO provide detailed information about the presence of intrinsic structural defects and nanorods in YBCO matrix as observed on cross-sectional BF-STEM images (figure 4). The growth of the nanorod in both films is different as nanorod length in 12BZO shows two types of nanorods: short (with the length of ≈ 16 nm) and long (≈ 47 nm), respectively, while 4BZO contains only one type nanorods with the length of ≈ 49 nm. The short nanorods of 16 nm in 12BZO are induced due to the presence of a great number of SFs, mostly between two nanorods and typically running through the whole film [58]. The 4BZO consists of SFs clearly less in number and they are mostly located between the nanorods and close to the YBCO/STO substrate interface. In addition, the BZO nanorod density is obviously different in these two samples, being roughly one third of the whole film volume in 4BZO and almost half of the volume in

Table 1. A compilation of general TEM results such as film thickness, SF length and distribution, and columnar ratio between YBCO and BZO columns in 4 wt.% and 12 wt.% BZO doped YBCO films.

Properties	4BZO	12BZO
Film thickness (nm)	240 ± 5.5	230 ± 6.5
SF length (nm)	39 ± 13.0	37 ± 10.0
SF	Next to interface	Whole film
YBCO/BZO column ratio	66%YBCO/34%BZO	53%YBCO/47%BZO

Table 2. The parameters of BZO nanorods measured from TEM images for 4 wt.% and 12 wt.% BZO doped YBCO films. The standard deviation of the values is around 10%.

BZO nanorods	Diameter (nm)	Length (nm)	Spacing (nm)	Splay (°)
4BZO	5.9	49.9	17.6	16
12BZO	5.4	16/47	5.6	10

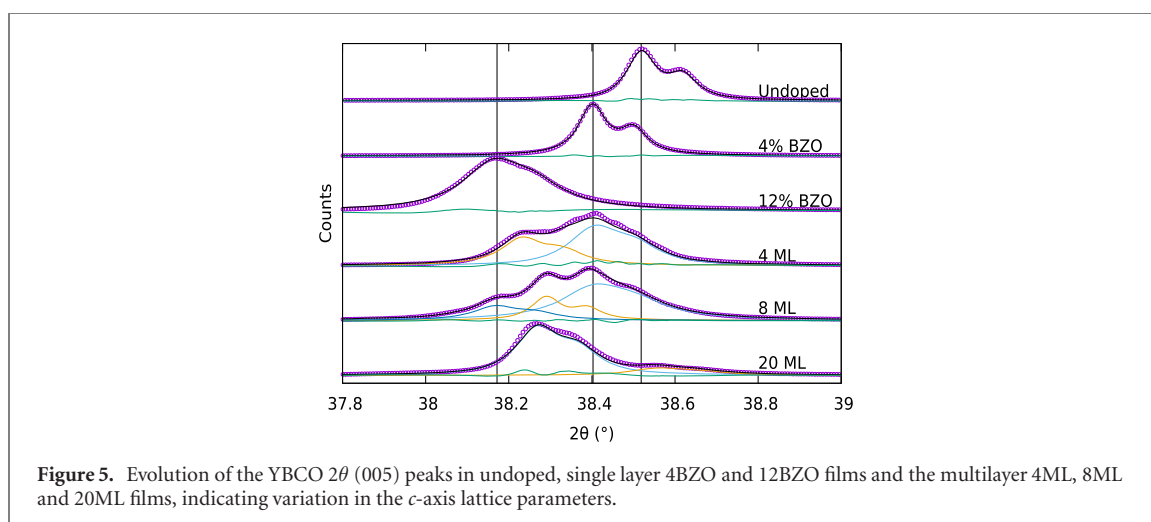
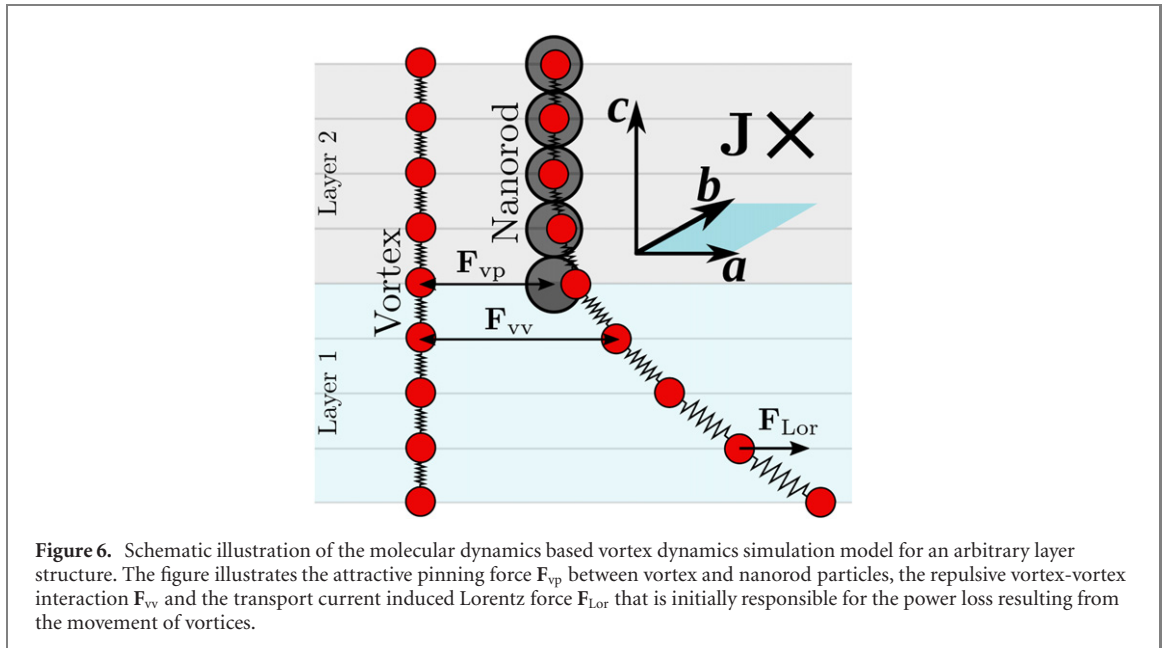


Figure 5. Evolution of the YBCO 2θ (005) peaks in undoped, single layer 4BZO and 12BZO films and the multilayer 4ML, 8ML and 20ML films, indicating variation in the c -axis lattice parameters.

12BZO film. This naturally leads to three times longer distance between the nanorods in 4BZO sample, while in 12BZO film, the distance between the outer edge of the nanorod is of the same order as the nanorod diameter. This means that 12BZO produces a maximum number of nanorods without starting to form too many other types of defects in the YBCO matrix. The most important structural indicators related to the YBCO films in general as well as to the BZO nanorods are given in tables 1 and 2, respectively. Although, the TEM data are for single layer films, our previous results [42] indicate that the APC structure remains similar within the multilayers with a sharp interface between the layers, as also observed in many other studies [27–30].

The structural properties of the deposited films analyzed by XRD show that BZO nanorods are epitaxially grown within the YBCO matrix. The details are given in SI. To determine the structural degradation of deposited single layer and multilayer films in comparison with an APC-free YBCO film, the details of the 2θ (005) diffraction peak structure were studied. As can be seen in figure 5, the 2θ peaks of both 4BZO and 12BZO single layers are shifted to lower 2θ value, being in line with our earlier results, where the BZO nanorods induced strain also lengthens the YBCO c -axis [35, 36]. However, the noticeable elongation of c -axis in 12BZO indicates significant increase of lattice strain, which degrades the YBCO structure by releasing the strain energy in this doping range [29, 35, 59]. On the other hand, the (005) diffraction peaks are composed of several sub-peaks, as clearly seen in multilayer films and the peak groups are situated between the peaks of single layer films of 4BZO and 12BZO. To get a clear picture of the respective components in multilayer films, the deconvolution of the (005) diffraction peak was carried out. As can be seen in figure 5, both the 4BZO and the 12BZO components are visible in the multilayer films, but their ratios vary greatly depending on the number and the thickness of the layers. For example in 4ML film, the 4BZO peak seems to dominate, which again indicates that each layer is thick enough to relax the growth of YBCO, whereas in 8ML the situation is more complex. In 20ML, each layer seems to be too thin,



for getting clearly separable YBCO layers with well defined unit cell structures. The in-plane and out-of-plane strain analysis from reciprocal space mapping measurement confirmed highly epitaxial growth in the in-plane direction and enhancement of preferred the out-of-plane direction with the broadened YBCO peak in q_z -direction especially in all multilayer films. This result is consistent with the rocking curves from ω -scans, the width of (005) peaks (see table S1, S1) are very similar for all multilayer films and thus the multilayering does not affect the direction appreciably. Based on these results, we can conclude that in comparison with 8ML and 20ML films, the 4ML film unambiguously demonstrates improved epitaxy and crystallinity, which can explain the observed great improvement in the $J_c(\theta)$ curves. This mechanism is thoroughly discussed in the following section.

4. Flux pinning mechanism in multilayers

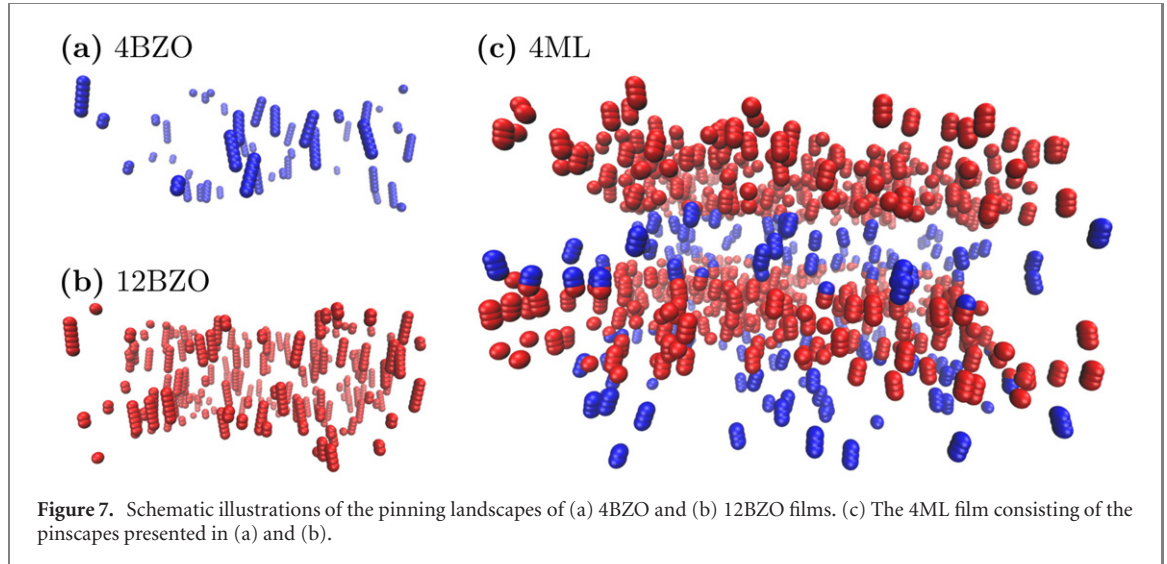
4.1. Critical current anisotropy simulations

The effect of nanorods on $J_c(\theta)$ via vortex pinning was further studied by running vortex dynamics simulations for nanorod lattices based on the BF measurements. The simulation model and the main acting forces are schematically illustrated in figure 6. The simulation model consists of two distinct types of particles, that are dynamic vortex particles that move according to Newtonian dynamics and immobile pinning site particles. A single vortex is modelled as a chain of individual vortex particles chained together via a spring-like tension force. The individual vortex particles are constrained in the c -direction into their own layers as illustrated in figure 6. The nanorod particles in the same layer repel each other according to the vortex-vortex interaction F_{vv} and are attracted to the pinning site particles via the pinning force F_{vp} . The vortex particles also experience the Lorentz F_{Lor} force that results from the applied transport current along with a drag force that ultimately causes the vortex dynamics induced power loss in the superconductor. The $J_c(\theta)$ was determined according to a stability condition of the vortex lattice. Thus, we want to point out that the simulation only considers the J_c that results from the stability of the vortices and does not take into account the associated intrinsic J_c of the material. The parameters of the corresponding nanorod lattices are presented in table 3 and schematically illustrated in figures 7(a) and (b). Further details of the molecular dynamics based simulation model are discussed in our previous papers [52, 60, 61].

The normalized simulated $J_c(\theta)$ curves for single layers of 4BZO and 12BZO doped YBCO are presented in figures 8(a) and (b). The shapes of the simulated $J_c(\theta)$ curves are in good agreement with the corresponding experimentally measured data presented in figure 2. The similarities between the experimental and simulated $J_c(\theta)$ for the 4BZO film are that for both cases, the c -peak is clearly present already in the low field range and can be observed to increase and sharpen as the field is increased up to 2 T. In the case of 12BZO film, the c -peak is almost absent in the low field range but it slowly increases as the field is increased. These results further validate the used simulation model for these systems and thus it may be used to analyze the corresponding 4ML structures.

Table 3. A summary of the parameters used in the simulation of $J_c(\theta, B)$ for layers of 4% and 12% BZO doped YBCO.

	4BZO	12BZO
Grid (abc)	150 nm \times 150 nm \times 60 nm	150 nm \times 150 nm \times 60 nm
Layers	30	30
Number of nanorods	41	186
Nanorod radius	2.95 nm	2.7 nm
Nanorod fragmentation	$c/5$	40% $c/14$ and 60% $c/5$
Nanorod splay	16°	10°



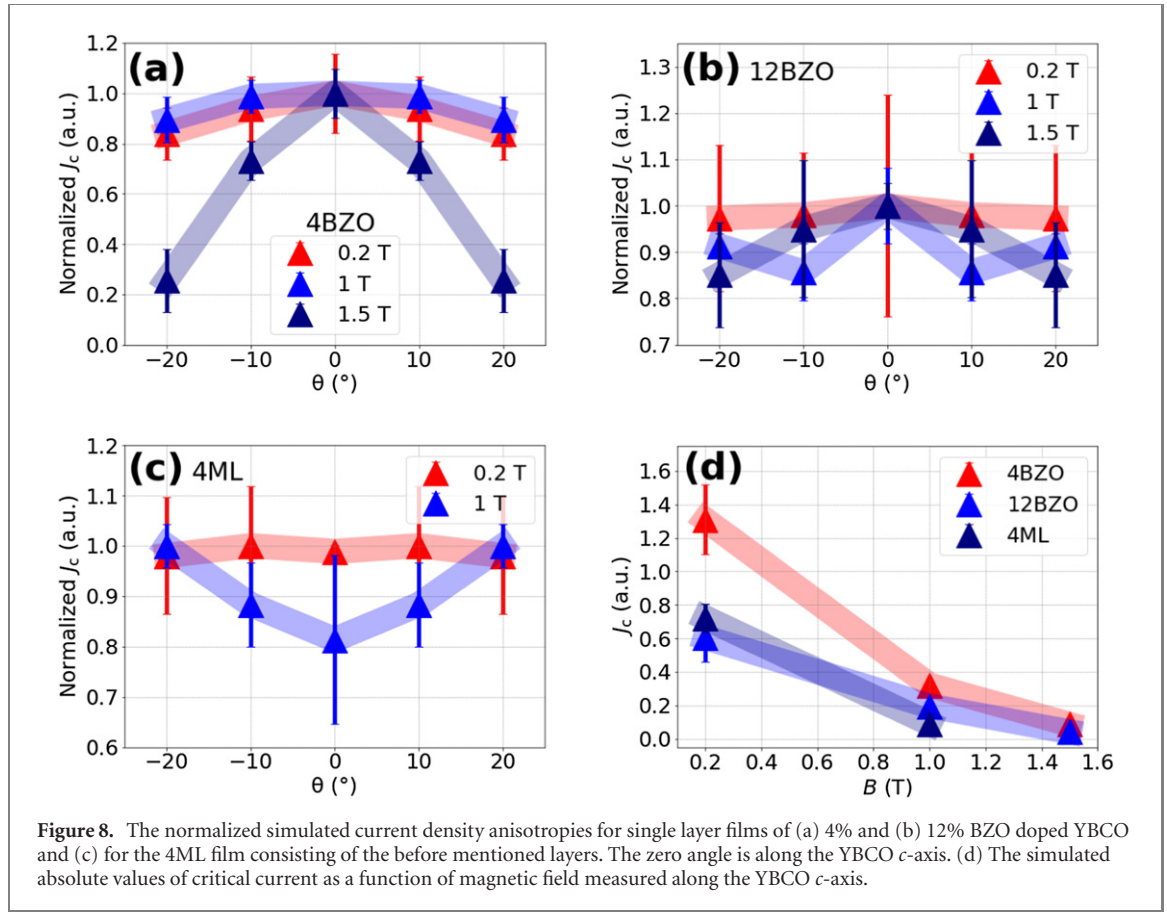
The $J_c(\theta)$ was simulated for the 4ML structure using a pinscape that consisted of four 30 nm thick layers mimicking the pinscapes used in the previously discussed single-layer simulation, as illustrated in figure 7(c). The normalized simulated $J_c(\theta)$ for this structure is presented in figure 8(c). Unfortunately, the $J_c(\theta)$ could not be reliably simulated above field of 1 T due to computational reasons. However, the shapes of the simulated $J_c(\theta)$ curves at 0.2 T and 1 T are again in good agreement with the corresponding experimentally measured $J_c(\theta)$ presented in figure 2 as the c -peak remains completely absent and the ab -peak broadens as the field is increased. Again, we conclude that the used simulation model is valid for analyzing the J_c determined by the stability of the vortex lattice. However, the simulated absolute values of J_c are inconsistent with the experiments.

The simulated absolute values of J_c along the YBCO c -axis as a function of field are presented in figure 8(d). One observes clear discrepancies by comparing the simulated $J_c(B)$ with the corresponding experimentally measured absolute values presented in figure 2. For example, the ratio of the simulated J_c s between the 4BZO and 12BZO decreases as a function of the field in contrast to the experimentally measured values. More interestingly, the simulated J_c of the 4ML structure at 0.2 T is significantly lower when compared with the single layer of 4BZO and, more remarkably, even lower when compared with the 12BZO case at 1 T. Since the utilized simulation model only considers the J_c according to the stability of the vortices, we conclude the fact that the experimentally measured J_c of the 4ML structure was observed to be superior at all fields, when compared with the single layer films, has to be related to highly increased $J_c(B = 0)$ of the 4ML film.

In the low field plateau of the $J_c(B)$ curve, the J_c is mostly determined by the crystalline quality of YBCO. Specifically, strain in very thin layers decreases $J_c(0)$ [62–64]. This suggests that the superior $J_c(B = 0)$ of the 4ML film, when compared with the corresponding single layer films along with the 8ML and 20ML films, could result from the improved general crystalline quality in terms of the reduced strain and number of various defects in the YBCO lattice. This assumption is supported by the XRD results, where crystallinity of YBCO is observed being greatly improved in 4ML film.

4.2. Improved crystalline quality of multilayer films

In order to quantitatively rationalize that the highly increased J_c of the 4ML film is due to reduced lattice strain, we turn to the widely used theory of film critical thickness (t_c) [65]. The critical thickness of a thin film is defined as the thickness above which it is energetically favourable for the lattice of the film to release



strain by forming dislocations. That is, above t_c the film becomes relaxed. The critical thickness can be evaluated using the formula

$$t_c = \frac{(1 - \nu \cos^2 \theta)b}{8\pi f(1 + \nu)} \ln \left(\frac{\beta t_c}{b} \right), \quad (1)$$

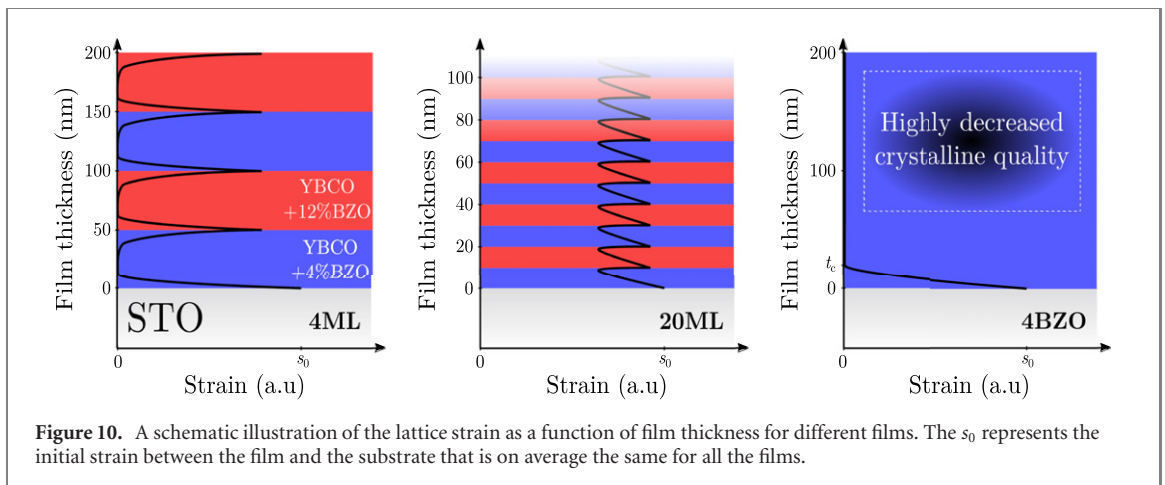
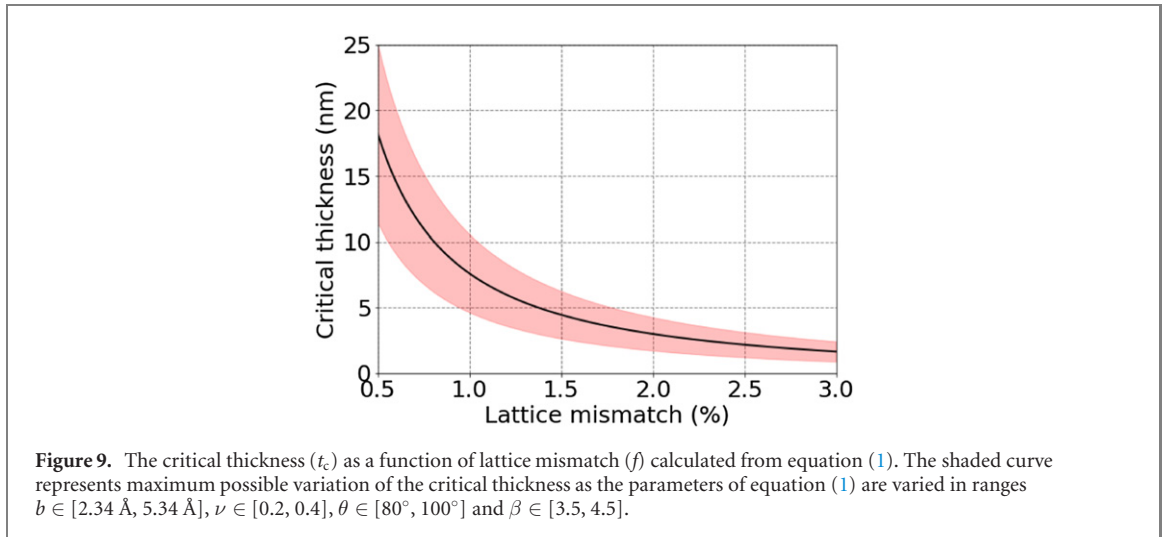
where f is the lattice mismatch between the film and the substrate, b is the magnitude of the Burgers vector of the dislocation, ν is the Poisson ratio of the film, θ is the angle between the Burgers vector and the dislocation line and β is the cutoff radius of the dislocation core [65]. The length scale of the Burgers vector is typically similar to the lattice parameters of the associated material. For YBCO, the average value of the a and b lattice parameters is $a_{\text{YBCO}} = 3.84 \text{ \AA}$ and the length of the Burgers vector can be assumed to be in the range of $b = a_{\text{YBCO}} \pm 2.5 \text{ \AA}$. The Poisson ratio of YBCO can be evaluated to range $\nu = 0.3 \pm 0.1$, while the parameter $\beta = 4 \pm 0.5$ is based on similar crystal systems [65–67]. The angle θ can be assumed to be in the range $\theta = 90^\circ \pm 10^\circ$. By using the aforementioned parameters, the t_c was numerically evaluated as a function of f as presented in figure 9.

In order to evaluate the critical thickness of the layer structure consisting of the 4BZO and 12BZO layers, it is convenient to define an effective lattice parameter of the doped material as

$$\bar{a} = \rho \cdot a_{\text{BZO}} + (1 - \rho) \cdot a_{\text{YBCO}}, \quad (2)$$

where $a_{\text{BZO}} = 4.17 \text{ \AA}$ is the lattice parameter of BZO and ρ is the corresponding nominal doping concentration. The effective lattice parameters for 4BZO and 12BZO cases can then be calculated as $\bar{a}_{4\%} = 3.85 \text{ \AA}$ and $\bar{a}_{12\%} = 3.88 \text{ \AA}$, respectively. The lattice mismatch $f = (\bar{a}_{4\%} - \bar{a}_{12\%})/\bar{a}_{4\%}$ of the corresponding layer structure is around 0.8%, suggesting a critical thickness of $\sim 10 \text{ nm}$ as evaluated from figure 9.

The average thickness of the deposited films can be evaluated to be around 200 nm. This means that the average thickness of a single layer is around 50 nm for the 4ML film and 10 nm for the 20ML film. Based on the previous calculation of the t_c , this suggests that the layer thickness of the 20ML film is too small for the strain of the lattice to relax unlike for the 4ML film and it is supported by the XRD results discussed in previous section. Thus, the 20ML film is on average much more strained which explains the deteriorated superconducting properties when compared with the 4ML film.



One could raise a concern about the above presented model, and is correct to do so, as it assumes that the growth of a new layer on top of an existing one is not affected by the strain relaxation of the existing layer. This assumption, however, seems to be more or less correct. In order to reason this, we remind that the growth process of the multilayer films required the interruption of the deposition for around two minutes as the target material was changed. We propose, that during this time period something happens to the surface of the film, which allows us to treat the upcoming layer of the film without considering the change of \bar{a} of the layer underneath. Although beyond the scope of this work, we suggest that during the change of the target, the surface of the film relaxes reducing the number of dislocations, thus improving the growth environment of the upcoming layers [25, 42, 68]. This proposal, although without any quantitative proof, explains well the observed results. The proposed lattice strain as a function of film thickness is schematically illustrated in figure 10.

With the earlier described assumption in mind, one can also explain why the 4ML film has superior J_c when compared with the single layer films, in particular to the 4BZO film. The lattice mismatch between STO and the 4BZO is around 1.4%, suggesting a critical thickness of only 5 nm according to figure 9. As the single layer films are around 200 nm thick, one would expect complete strain relaxation for over 97% of the interior of the film and thus much higher J_c when compared with the 4ML film. The discrepancy between the aforementioned statement and the experimental results suggests that the decreased J_c of the single layer films is due to highly reduced crystalline quality resulting from the increased number of dislocations as the thickness of the film increases [69, 70]. Unlike the multilayer films, the single layer films were deposited in a single setting without any breaks during the deposition. Thus, the adatoms on the surface of the film do not have time enough to diffuse into the minimum energy positions, inducing dislocations and other defects as the film grows. The increased number of dislocations aggravates the affiliation of new unit cells to the surface, leading to the rapid decay in crystalline quality as the thickness of the film increases, as illustrated in figure 10. This is manifested for example as increasing surface roughness of the film as a function of thickness [71]. Thus, despite their reduced strain, the single layer films can be expected to have on average

much worse crystalline quality when compared with the 4ML film. These suggestions fit perfectly with the experimental results and the critical thickness theory. The theory is also in line with the fact that all of the multilayer structures obtain remarkably higher values of J_c in the high field range, as the superconducting properties are highly dependent in particular on the crystalline quality of the film that was deduced to be on average remarkably reduced for the 200 nm thick single layer films [72, 73].

Based on the results and the discussion above, it is clear that by multilayering the superconducting films one is able to remarkably increase the J_c , especially in the high temperature and field ranges. For applications working in particular under high magnetic fields, where the multilayering was deduced to be most effective, controlling the vortex movement by doping of the superconducting material is a necessity. For this reason, the possibility of intrinsic layers was not considered in this work.

5. Conclusions

In this work, we have grown superconducting YBCO single layer films together with multilayer structures by depositing the alternating BZO doped YBCO layers of various layer thicknesses with different BZO nanocolumn densities. Our results based on detailed structural analyses by x-ray diffractometry and transmission electron microscopy indicate that the layer thickness strongly affects on the intrinsic superconducting and the flux pinning properties, which together have an extremely critical role in formation of the optimal critical current densities in different external magnetic field and temperature ranges. The experimental results are verified with the vortex dynamics simulations and widely addressed with the theories of the critical thicknesses of the layers. Based on these discussions, we have demonstrated a general model for the HTS multilayers, where by varying the layer thickness and the dopant nanorod density, it is possible to produce a greatly improved vortex pinning structure. The presented YBCO multilayer, with the combination of optimal $J_c(0)$ and $J_c(B)$, leads to as high critical current density as possible needed in the desired application working at different magnetic fields.





Acknowledgments

The Jenny and Antti Wihuri Foundation and the University of Turku Graduate School are acknowledged for financial support. Hannes Rijckaert acknowledges support and funding as postdoctoral fellow fundamental research of the Research Foundation-Flanders (FWO, Grant No. 1273621N). The computer resources of the Finnish IT Center for Science (CSC) and the FGCI project (Finland) are acknowledged.

Data availability statement

All data that support the findings of this study are included within the article (and any supplementary files).

ORCID iDs

Moe M Aye  <https://orcid.org/0000-0001-8021-118X>
Elmeri Rivasto  <https://orcid.org/0000-0002-1255-0726>
Mukarram Z Khan  <https://orcid.org/0000-0001-6903-2308>
H Rijckaert  <https://orcid.org/0000-0002-6078-2919>
H Huhtinen  <https://orcid.org/0000-0002-2166-5939>
Isabel Van Driessche  <https://orcid.org/0000-0001-5253-3325>
P Paturi  <https://orcid.org/0000-0002-6240-2801>

References

- [1] Foltyn S R, Civalo L, MacManus-Driscoll J L, Jia Q X, Maiorov B, Wang H and Maley M 2007 *Nat. Mater.* **6** 631–42
- [2] Holesinger T G et al 2008 *Adv. Mater.* **20** 391–407
- [3] Obradors X and Puig T 2014 *Supercond. Sci. Technol.* **27** 044003
- [4] Larbalestier D, Gurevich A, Feldmann D M and Polyanskii A 2001 *Nature* **414** 368–77
- [5] Civalo L et al 2004 *Appl. Phys. Lett.* **84** 2121–3
- [6] Kang S et al 2006 *Science* **311** 1911–4
- [7] Wee S H, Goyal A, Zuev Y L and Cantoni C 2008 *Supercond. Sci. Technol.* **21** 092001
- [8] Matsumoto K and Mele P 2010 *Supercond. Sci. Technol.* **23** 014001
- [9] Goyal A et al 2005 *Supercond. Sci. Technol.* **18** 1533–8

- [10] Maiorov B, Baily S A, Zhou H, Ugurlu O, Kennison J A, Dowden P C, Holesinger T G, Foltyn S R and Civale L 2009 *Nat. Mater.* **8** 398–404
- [11] Baca F J, Haugan T J, Barnes P N, Holesinger T G, Maiorov B, Lu R, Wang X, Reichart J N and Wu J Z 2013 *Adv. Funct. Mater.* **23** 4826–31
- [12] Wee S H, Zuev Y L, Cantoni C and Goyal A 2013 *Sci. Rep.* **3** 23101–9
- [13] Jha A K, Matsumoto K, Horide T, Saini S, Mele P, Ichinose A, Yoshida Y and Awaji S 2016 *IEEE Trans. Appl. Supercond.* **26** 8000404
- [14] Wu J Z, Shi J J, Baca F J, Emergo R, Wilt J and Haugan T J 2015 *Supercond. Sci. Technol.* **28** 125009
- [15] Horide T, Kawamura T, Matsumoto K, Ichinose A, Yoshizumi M, Izumi T and Shiohara Y 2013 *Supercond. Sci. Technol.* **26** 075019
- [16] Foltyn S R, Wang H, Civale L, Jia Q X, Arendt P N, Maiorov B, Li Y, Maley M P and MacManus-Driscoll J L 2005 *Appl. Phys. Lett.* **87** 162505
- [17] Haugan T, Barnes P N, Wheeler R, Meisenkothen F and Sumption M 2004 *Nature* **430** 867
- [18] Barnes P N, Haugan T J, Varanasi C V and Campbell T A 2004 *Appl. Phys. Lett.* **85** 4088
- [19] Campbell T A, Haugan T J, Maartense I, Murphy J, Brunke L and Barnes P N 2005 *Physica C* **423** 1
- [20] Matsumoto K, Horide T, Mele P, Yoshida Y, Mukaida M, Ichinose A and Horii S 2005 *Physica C* **426–431** 1091
- [21] Gapud A A, Kumar D, Viswanathan S K, Cantoni C, Varela M, Abiade J, Pennycook S J and Christen D K 2005 *Supercond. Sci. Technol.* **18** 1502
- [22] Cai C, Hänisch J, Hühne R, Stehr V, Mickel C, Gemming T and Holzapfel B 2005 *J. Appl. Phys.* **98** 123906
- [23] Sueyoshi T, Watanabe M, Haruta M, Fujiyoshi T, Miyahara K, Ikegami T, Ebihara K and Miyagawa R 2008 *Physica C* **468** 1266
- [24] Jia Q X, Foltyn S R, Arendt P N and Smith J F 2002 *Appl. Phys. Lett.* **80** 1601
- [25] Huhtinen H, Schlesier K and Paturi P 2009 *Supercond. Sci. Technol.* **22** 075019
- [26] Haugan T J, Barnes P N, Campbell T A, Pierce N A, Baca F J and Maartense I 2007 *IEEE Trans. Appl. Supercond.* **17** 3724
- [27] Kobayashi H, Yamada Y, Ibi A, Miyata S, Shiohara Y, Kato T and Hirayama T 2007 *Physica C* **463–465** 661–4
- [28] Kang S, Leonard K J, Martin P M, Li J and Goyal A 2007 *Supercond. Sci. Technol.* **20** 11
- [29] Ichinose A, Naoe K, Horide T, Matsumoto K, Kita R, Mukaida M, Yoshida Y and Horii S 2007 *Supercond. Sci. Technol.* **20** 1144–50
- [30] Matsumoto K, Tanaka I, Horide T, Mele P, Yoshida Y and Awaji S 2014 *J. Appl. Phys.* **116** 163903
- [31] MacManus-Driscoll J L et al 2004 *Nat. Mater.* **3** 439
- [32] Yamada Y et al 2005 *Appl. Phys. Lett.* **87** 132502
- [33] Mele P, Matsumoto K, Ichinose A, Mukaida M, Yoshida Y, Horii S and Kita R 2008 *Supercond. Sci. Technol.* **21** 125017
- [34] Augieri A et al 2008 *J. Phys.: Conf. Ser.* **97** 012209
- [35] Peurla M, Paturi P, Stepanov Y P, Huhtinen H, Tse Y Y, Bódi A C, Raittila J and Laiho R 2006 *Supercond. Sci. Technol.* **19** 767–71
- [36] Peurla M, Huhtinen H, Tse Y Y, Raittila J and Paturi P 2007 *IEEE Trans. Appl. Supercond.* **17** 3608–11
- [37] Pompeo N, Galluzzi V, Augieri A, Fabbri F, Celentano G, Petrisor T, Rogai R and Silva E 2008 *J. Phys.: Conf. Ser.* **97** 012173
- [38] Baca F J, Barnes P N, Emergo R L S, Haugan T J, Reichart J N and Wu J Z 2009 *Appl. Phys. Lett.* **94** 102512
- [39] Emergo R L S, Baca F J, Wu J Z, Haugan T J and Barnes P N 2010 *Supercond. Sci. Technol.* **23** 115010
- [40] Wang X, Baca F J, Emergo R L S, Wu J Z, Haugan T J and Barnes P N 2010 *J. Appl. Phys.* **108** 113911
- [41] Liu Y and Du G 2011 *J. Electron. Mater.* **40** 1512–6
- [42] Malmivirta M, Rijckaert H, Paasonen V, Huhtinen H, Hynninen T, Jha R, Awana V S, van Driessche I and Paturi P 2017 *Sci. Rep.* **7** 14682
- [43] Blatter G, Feigel'man M V, Geshkenbein V B, Larkin A I and Vinokur V M 1994 *Rev. Mod. Phys.* **66** 1125–388
- [44] Matsushita T 2007 *Flux Pinning in Superconductors* (Heidelberg: Springer)
- [45] Yang H et al 2009 *J. Appl. Phys.* **106** 093914
- [46] Zhao R et al 2014 *Adv. Funct. Mater.* **24** 5240–5
- [47] Raittila J, Huhtinen H, Paturi P and Stepanov Y P 2002 *Physica C* **371** 90–6
- [48] Huhtinen H, Järvinen J, Laiho R, Paturi P and Raittila J 2001 *J. Appl. Phys.* **90** 1521–8
- [49] Rijckaert H et al 2017 *Chem. Mater.* **29** 6104–13
- [50] Wiesinger H P, Sauerzopf F M and Weber H W 1992 *Physica C* **203** 121–8
- [51] Malmivirta M, Yao L D, Huhtinen H, Palonen H, van Dijken S and Paturi P 2014 *Thin Solid Films* **562** 554–60
- [52] Khan M Z et al 2019 *Sci. Rep.* **9** 15425
- [53] Aye M M, Khan M Z, Rivasto E, Tikkanen J, Huhtinen H and Paturi P 2019 *IEEE Trans. Appl. Supercond.* **29** 8000805
- [54] Develos-Bagarinao K, Yamasaki H and Ohki K 2008 *J. Appl. Phys.* **104** 063907
- [55] Cai C, Holzapfel B, Hänisch J and Schultz L 2004 *Phys. Rev. B* **70** 212501
- [56] Pan A V, Pysarenko S V, Wexler D, Rubanov S, Ionescu M and Dou S X 2007 *Physica C* **460–462** 1379
- [57] Khan M Z et al 2021 *ACS Cryst. Growth Des.* (under review)
- [58] Horide T, Ishimaru M, Sato K and Matsumoto K 2020 *Supercond. Sci. Technol.* **33** 115001
- [59] Huhtinen H, Irjala M, Paturi P, Shakhov M A and Laiho R 2010 *J. Appl. Phys.* **107** 053906
- [60] Paturi P, Malmivirta M, Hynninen T and Huhtinen H 2018 *J. Phys.: Condens. Matter* **30** 315902
- [61] Rivasto E, Khan M Z, Malmivirta M, Rijckaert H, Aye M M, Hynninen T, Huhtinen H, Driessche I V and Paturi P 2020 *Sci. Rep.* **10** 3169
- [62] Zhai H Y and Chu W K 2000 *Appl. Phys. Lett.* **76** 3469
- [63] Varela M, Grogger W, Arias D, Sefrioui Z, León C, Vazquez L, Ballesteros C, Krishnan K M and Santamaría J 2002 *Phys. Rev. B* **66** 174514
- [64] Li Z, Coll M, Mundet B, Palau A, Puig T and Obradors X 2020 *Nanoscale Adv.* **2** 3384–93
- [65] He J, Klie R F, Logvenov G, Bozovic I and Zhu Y 2007 *J. Appl. Phys.* **101** 073906
- [66] Schulman A, Palonen H, Lähteenlahti V, Beiranvand A, Huhtinen H and Paturi P 2020 *J. Phys.: Condens. Matter* **33** 035803
- [67] Sandiumenge F, Santiso J, Balcells L, Konstantinovic Z, Roqueta J, Pomar A, Espinós J P and Martínez B 2013 *Phys. Rev. Lett.* **110** 107206
- [68] Benzi P, Bottizzo E and Rizzi N 2004 *J. Cryst. Growth* **269** 625–9
- [69] Matsushita T, Kiuchi M, Kimura K, Miyata S, Ibi A, Muroga T, Yamada Y and Shiohara Y 2005 *Supercond. Sci. Technol.* **18** 227
- [70] Zhang H, Yang J, Wang S, Wu Y, Lv Q and Li S 2014 *Physica C* **499** 54–6
- [71] Huhtinen H, Irjala M, Paturi P and Falter M 2012 *Physica C* **472** 66–74

- [72] Rostila L, Lehtonen J and Mikkonen R 2007 *Physica C* [451 66–70](#)
- [73] Shin H-S, Kim K-H, Dizon J R C, Kim T-Y, Ko R-K and Oh S-S 2005 *Supercond. Sci. Technol.* [18 S364](#)